ELSEVIER

Tectonophysics 327 (2000) 131–148

TECTONOPHYSICS

www.elsevier.com/locate/tecto

Determination of deviatoric stress tensors based on inversion of calcite twin data from experimentally deformed monophase samples. Part II. Axial and triaxial stress experiments

Ph. Laurent[a,*], H. Kern[b], O. Lacombe[c]

[a]*Laboratoire de Tectonique et Géophysique, Université de Montpellier II, Place E. Bataillon, 34095 Montpellier Cedex, France*
[b]*Mineralogisch–Petrographisches Institut der Universität Kiel, Kiel, Germany*
[c]*Laboratoire de Tectonique Quantitative, ESA 70-72, CNRS, Université Pierre et Marie Curie, 75252 Paris Cedex O5, France*

Received 7 January 2000; accepted 3 July 2000

Abstract

Three samples of a bioclastic bajocian limestone from Burgundy (France) were experimentally deformed under axial and triaxial conditions at 200 and 300°C. In each sample, a series of three mutually orthogonal thin sections were studied using a U stage. The intracrystalline deformation of the calcite grains involved mainly twinning on the *e* planes. Precise measurement of the *e* twin lamellae combined with the Etchecopar inverse method (1984) allowed the calculation of the four parameters of the reduced stress tensor responsible for the twinning. As the principal differential stress values of the experimental deviatoric stress tensors were known, the critical resolved shear stress (CRSS) values τ_s for twinning on the *e* planes were then determined in each case: at 200°C and 4.8% strain, τ_s is close to 15 MPa; at 300°C and at 8.7 and 9.4% strain, the calculated τ_s values are close to 10.1 and 13.4 MPa, respectively. When compared with the data published by Turner et al. (1954), Turner and Heard (1965) and Lacombe and Laurent (1996), our results confirm that the CRSS values are more or less dependent on both the temperature and the bulk amount of strain. Consequences for the estimation of the actual principal differential stress values ($\sigma_1 - \sigma_3$) are described, particularly for very weakly deformed cover rocks in the forelands of mountain chains.

Keywords: triaxial tests; calcite; twins; shear stress

1. Introduction

During the last two decades, several studies have dealt with the characterization of present or ancient stress states in cratonic areas and in the foreland of mountain chains (e.g. Engelder and Geiser, 1980; Zoback et al., 1989; Zoback, 1992; Craddock et al., 1993; Arthaud and Laurent, 1995; Lacombe et al., 1996; Van Der Pluijm et al., 1997). In sedimentary rocks of the shallow crust, carbonate rocks are probably the most useful for studying brittle deformation and associated stresses. This is partly due to the efficiency of the pressure-solution process in carbonate rocks and partly to the ability of calcite crystals to deform easily at low temperature by twinning on the *e* planes {01.2} (Baumhauer in Friedel (1926)). Although these two mechanisms and faulting both contribute to the bulk strain rate, calcite twin analysis can be considered to provide a good estimate of the peak of actual differential stresses (Rowe and Rutter, 1990; Lacombe and Laurent, 1992).

* Corresponding author. Fax: +33-4-6752-3908.
E-mail address: laurent@dstu.univ-montp2.fr (P. Laurent).

0040-1951/00/$ - see front matter
PII: S0040-1951(00)00165-7

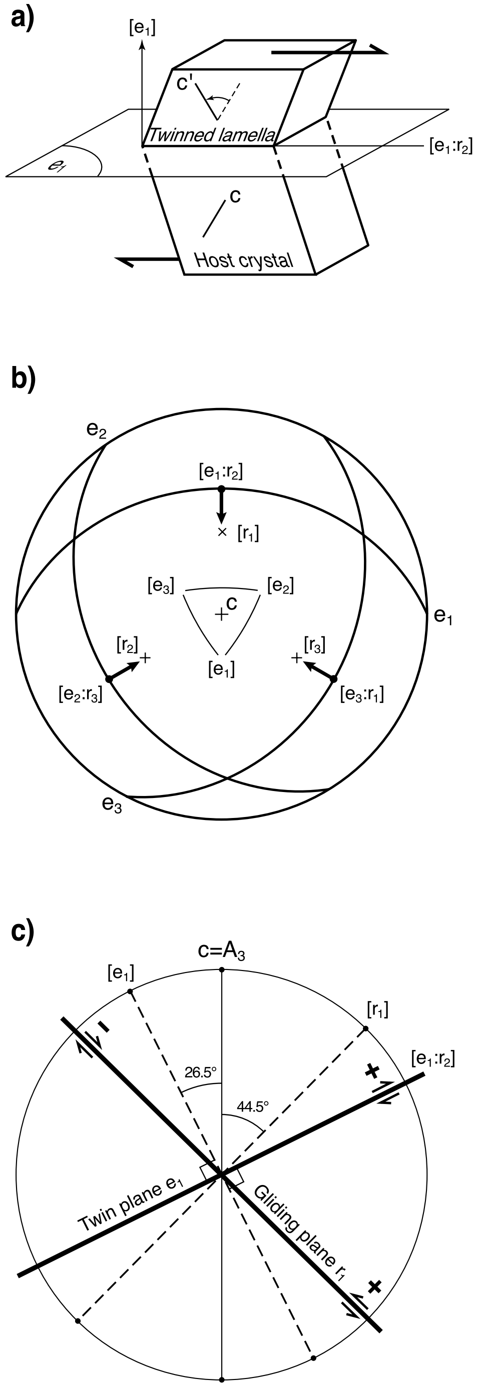

Fig. 1. Geometry of twinning on the *e* planes in calcite. (a) Schematic drawing of one e_1 twinned lamella [10.2]. *C* is the optical axis [00.1], i.e. the ternary axis of symmetry (A_3) of the calcite host crystal. The normal to the plane of twinning is [e_1]; the direction of twinning is [e_1:r_2]; the imposed sense of shear is indicated by the arrows: by convention, this sense is defined as positive. After twinning, the twinned lamella, which is generally very thin (about a portion of micron), is symmetrical of the host crystal with respect to the twin plane e_1; C' is the optical axis of the twinned lamella. Note that the optical axis (C–C′) rotates in the opposite direction to the lamella. (b) Stereographic projection (lower hemisphere, equal area), of some of the principal planes of the calcite crystal. The optical axis *C* is vertical at the center of the diagram. The poles to the three sets of twin planes are [e_1], [e_2] and [e_3]. The planes of twinning e_i are the large circles; they contain the twinning direction [e_i : r_j]; for each twin plane, the arrow is parallel to the twinning direction; its head indicates that the upper part of the crystal moves upward, toward the *C* axis, as a reverse microfault. The poles to the three sets of cleavage planes (and gliding planes) r_j are [r_1], [r_2] and [r_3]. (c) The sense of shear on e_1 and r_1, viewed in the plane perpendicular to both e_1 and r_1. This plane contains the optical axis *C*, and the poles [e_1], and [r_1]. On e_1, the positive sense of shear, as defined by the arrows, is the only one possible. On r_1, both the positive and negative sense of shear are equally possible.

Following on from Lacombe and Laurent (1996), we tackled two key points related to the determination of the magnitudes of the differential stresses using calcite twin inverse analyses in carbonate rocks. (1) The critical resolved shear stress (CRSS) value τ_s for twinning on the *e* planes at low temperatures. Using inverse methods, this parameter is necessary to compute the principal differential stress $(\sigma_1 - \sigma_3)$ of the deviatoric stress tensor (DST) responsible for the observed twinning. (2) The determination of the stress ellipsoid shape ratio (SESR) $\Phi = (\sigma_2 - \sigma_3)/(\sigma_1 - \sigma_3)$, when the state of stress is actually triaxial (plane strain conditions). This second parameter is necessary to compute the differential stress values $(\sigma_2 - \sigma_3)$ and $(\sigma_1 - \sigma_2)$. Up to now, these two parameters have been poorly constrained by experimental work under low temperature conditions, although they are essential when considering brittle deformation.

2. Tectonic analysis of calcite twin lamellae

Fig. 1 summarizes the geometry of calcite twinning on the *e* planes. For more details, see Cahn (1954), Carter and Raleigh (1969), Friedman (1967) and Barber and Wenk (1979). At low temperature, the *e* twin lamellae are thin and straight (Burkhard, 1993) and may be compared to reverse microfaults when the C axis of the calcite crystal [0001] is oriented vertically (Fig. 1b). Then, the direction, the sense of shear and the shear strain associated with twinning are all constrained by the calcite crystal.

After the pioneering work of Turner (1953), several methods for determining stress or strain from calcite twin lamellae were proposed. A recent review exists on this topic (Burkhard, 1993), so, these methods will not be recalled here. For stress determinations, one must distinguish three basically different approaches.

In the first method, only the principal axes of the incremental strain tensor, i.e. the P and T axes (see discussion in Marrett and Peacock, 1999) are determined (e.g. Turner, 1953, 1962). This method is theoretically justified for monophase deformation if the stress is axial. Numerous applications to experimental and geological deformation have demonstrated the efficiency of Turner's method (e.g. Friedman and Stearns, 1971; Friedman et al., 1976).

In the second method, only the absolute magnitude of the principal differential stress $(\sigma_1 - \sigma_3)$ is determined (e.g. Friedman and Heard, 1974; Jamison and Spang, 1976; Schmid, 1982; Rowe and Rutter, 1990). This is an advantage of calcite twin lamellae analysis as the magnitude of differential stresses $(\sigma_i - \sigma_j)$ in the Earth's crust is of central importance for earth scientists. Quantification of the principal differential stress $(\sigma_1 - \sigma_3)$ is made possible by the use of different experimental data from calcite monocrystals or polycrystals such as the twin/grain size dependence (Schmid, 1982), the twinning incidence (percentage of twinned grains with a given grain size), the twin density or volume (Rowe and Rutter, 1990), or a constant threshold value τ_s equal to the CRSS for twinning on the e planes. For low temperature deformation, the accepted τ_s value is 10 MPa (e.g. Turner and Heard, 1965; Jamison and Spang, 1976; Tullis, 1980). Nevertheless, it is well known that twinning is more or less dependent on grain size, temperature, and stress heterogeneity (Turner et al., 1954; Olsson, 1974; Spiers, 1979; Tullis, 1980; Schmid, 1982; Rowe and Rutter, 1990; Wheeler, 1991; Newman, 1994; De Bresser and Spiers, 1997). Ferrill (1998) recently used the Jamison and Spang (1976) and Rowe and Rutter (1990) methods to estimate the principal differential stress magnitudes for limestones deformed experimentally and naturally at low temperatures. Overestimation by a factor of up to 20 was obtained and Ferrill concluded that the use of a constant τ_s value is a "key weakness" of these methods.

Lastly, other methods involve the calculation of the whole DST. The DST is defined by five parameters that may be described as the three principal stress orientations and two values of the differential stresses $(\sigma_i - \sigma_j)$ (Laurent et al., 1981, 1990). Application of these methods depends upon several assumptions: (1) The homogeneous state of stress at the scale of the thin section; i.e. the five parameters of the DST are constant on this scale. (2) Coaxial deformation on the same scale. (3) Low strain (a few percent) at low temperature. These conditions require that the dominant intracrystalline deformation mechanism is twinning on the e planes (Turner et al., 1954; De Bresser and Spiers, 1993, 1997), and no rotation of grains is possible. (4) Samples are made of euhedral calcite grains with no crystallographic preferred orientation. (5) Mechanical twinning is independent of normal stress. Twinning takes place on a given e plane, if and only if the resolved shear stress along the twinning direction $[e_i : r_j]$, in the positive sense (Fig. 1c) is greater than a positive value defined as the CRSS for twinning on the e planes. The validity of these assumptions was discussed by Wenk et al. (1983), Burkhard (1993) and Lacombe and Laurent (1996).

3. The inverse Etchecopar method (1984)

The inverse Etchecopar method (Etchecopar, 1984; Laurent, 1984; Lacombe and Laurent, 1996) is very similar to that used to determine the reduced stress tensor (RST) associated with striated faults sets (Etchecopar et al., 1981). The RST are defined by only four parameters (Angelier, 1984, 1989) which are the three principal stress orientations and the stress ellipsoid shape ratio (SESR) $\Phi = (\sigma_2 - \sigma_3)/(\sigma_1 - \sigma_3)$. Basically, for striated fault analyses, the use of the RST for calcite twins is justified, primarily for two reasons: first, it was shown that the four parameters of the RST are sufficient to determine uniquely the direction and sense of shear on a given plane (Wallace, 1951; Bott, 1959). Second, the calculation process is

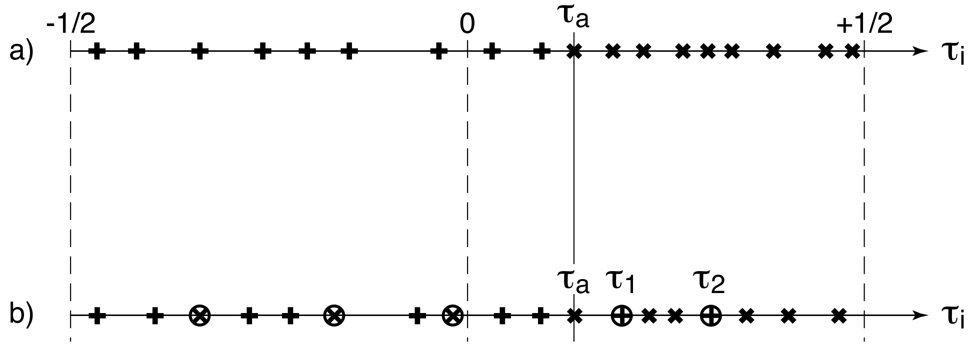

Fig. 2. Schematic classification of the *e* planes, with respect to the applied resolved shear stress τ_i, by the Etchecopar inverse method. Six crystals are considered (18 *e* planes); 9 *e* planes (50%) are twinned. The applied resolved shear stress τ_i increases to the right of the figure, from $-1/2$ to $+1/2$. τ_a is the lowest resolved shear stress applied on the compatible twinned planes. ($\times$) Compatible twinned planes; (+) compatible untwinned planes; ($\otimes$) incompatible twinned planes; ($\oplus$) incompatible untwinned planes. (a) Theoretical situation: 100% of twinned planes are compatible with the RST. Then, the function of penalization F is equal to 0. (b) Example of actual situation: 6 twinned planes (67%) are compatible with the RST; 2 untwinned planes (22%) are incompatible with the RST. The function of penalization F is equal to $(\tau_1 - \tau_a) + (\tau_2 - \tau_a)$.

made easier with only four parameters. We point out that the RST is not a deviatoric stress tensor, as the principal stress values are, respectively: $\sigma_1 = 1$, $\sigma_2 = \Phi$ and $\sigma_3 = 0$. A simple calculation leads to the deviatoric part of the RST. Thus, it is possible to determine the actual DST by introducing a scaling parameter, namely the CRSS for twinning τ_s, which is supposedly constant for all the calcite grains. The actual differential stress values $(\sigma_i - \sigma_j)$ are then proportional to τ_s.

This method makes use of the whole measured *e* planes data set (twinned and untwinned planes), without any separation prior to the stress inversion (Nemcock et al., 1999). We restate this method briefly only for monophase deformation (for more details, see Etchecopar, 1984). For polyphase deformation, the procedure is the same as that used for striated faults set analysis (see Etchecopar et al., 1981).

The problem is to find an RST which satisfies both the following conditions: (1) For each twin plane, the applied resolved shear stress τ_i is positive, as defined by Turner (1953) see Fig. 1, and greater than or equal to a critical positive value τ_a. As $(\sigma_1 - \sigma_3)$ is scaled to unity by the RST, the τ_i values lie somewhere between $+1/2$ and $-1/2$. Then, the τ_a value corresponds to the actual CRSS value; τ_s divided by $(\sigma_1 - \sigma_3)$; it lies somewhere between 0 and $+1/2$ (Fig. 2). (2) For each untwinned plane, τ_i must be lower than τ_a.

First, a great number of RSTs (500 or more) are defined using randomly chosen parameters. The application of all these RSTs to the twin data set allows the calculation of the τ_i values acting on each *e* plane. Then, for each RST, all the *e* planes are classified according to their τ_i values (Fig. 2). The ideal solution, if it exists, is that for which all the *e* planes (twinned and untwinned) are classified as shown in Fig. 2a. Obviously, natural samples never fit the theoretical limits and Fig. 2b shows a more realistic classification of the *e* planes when natural deformation is analyzed.

Thus, four situations may be considered: (1) the compatible twinned planes for which $\tau_i \geq \tau_a$ are on the right side of the diagram in Fig. 2b labeled with $\times$; (2) the incompatible twinned planes, for which $\tau_i < \tau_a$ is labeled with $\otimes$; (3) the compatible untwinned planes for which $\tau_i < \tau_a$ is labeled with $+$; (4) the incompatible untwinned planes for which $\tau_i > \tau_a$ is labeled with $\oplus$. This last set of *e* planes is very important for the calculation of the RST, because the penalization function F of Etchecopar (1984) which is used to define the best solution, is calculated as the sum of the $(\tau_i - \tau_a)$ values for all the *n* incompatible untwinned planes

$$F = \sum_{i=1}^{i=n} (\tau_i - \tau_a) \quad (1)$$

For the ideal case of Fig. 2a, F is equal to 0. For actual

Table 1
Experimental conditions

	B21	B31	B32
Strain ellipsoid	Axial: $\epsilon_2 = \epsilon_3$	Axial: $\epsilon_2 = \epsilon_3$	Triaxial: $\epsilon_2 = 0$
Temperature (°C)	201 ± 1	305 ± 1	305 ± 1
Confining pressure σ_3 (MPa)	100–102	200–213	200–221
Isotropic pressure (MPa)	100–185	200–302	200–372
Final σ_1 (MPa)	350	480	537
Final σ_2 (MPa)	102	213	359
Maximum of $(\sigma_1 - \sigma_3)$	248	267	316
SESR Φ	0	0	0–0.43
Final linear strain ϵ_1 (%)	−4.83	−8.73	−9.38
Final linear strain ϵ_2 (%)	1.77	2.76	0
Final linear strain ϵ_3 (%)	1.84	2.91	5.3
Maximum of $\Delta V/V$ (%)	−1.4	−3.5	−4.6
Strain rate (10^{-6} s^{-1})	1.8	1.4	1.4

cases, the F values are positive and depend on the applied RSTs. For the example shown in Fig. 2b, $F = (\tau_1 - \tau_a) + (\tau_2 - \tau_a)$. The RST for which F is minimized, yields a first estimate of the best solution, generally quite close to it (see below).

The second step of the Etchecopar method is an optimization process and a refinement of the solution, the same as for striated faults sets analyses. This is done by using a fast nonlinear optimizing procedure, which proceeds by steps in the parameter space. For details, see Etchecopar et al. (1981).

Obviously, the RST calculation must be independent of the incompatible twinned planes. Therefore, the Etchecopar inverse method requires a parameter P which represents the percentage of compatible twins with respect to the whole measured twinned planes set. Because this P value is unknown, several trials are carried out.

4. Previous results

To date, the Etchecopar inverse method has been applied to experimental and mainly to natural deformations (e.g. Larroque and Laurent, 1988; Tourneret and Laurent, 1990; Lacombe et al., 1991, 1992, 1993, 1996; Lacombe and Laurent, 1992). Three points emerge from a critical review of this work:

(1) The principal stress orientations are relatively well defined, even when the deformation is polyphased (e.g. Lacombe et al., 1990a,b, 1992, 1996). Nevertheless, as pointed out by some authors (Burkhard, 1993; Nemcock et al., 1999), a more or less important set of twinned planes (about 5–40%) is generally rejected by the computing process. Without any additional information, it was concluded that these twin sets should correspond to primary twins or to twins created in a locally different stress field. Secondly, additional stress tensors with respect to other microstructural methods are generally determined using calcite twins (e.g. sample from Taxenne in the Fig. 10 of Lacombe et al., 1990b). This result, which is not characteristic of the Etchecopar inverse method (e.g. Gonzalez-Casado and Garcia-Cuevas, 1999), may result from the ease of twinning on the best oriented calcite grains.

(2) The inverse determination of the SESR is more difficult to appreciate for two main reasons: First, the previous experimental work used (Laurent, 1984; Lacombe and Laurent, 1996) always dealt with axial deformation, with $\Phi = 0$. Second, for applications to geological deformations, it is rather risky to compare the results obtained with calcite twins inverse methods to those obtained with striated faults inverse methods (see discussion in Lacombe et al., 1990b, 1992).

(3) The principal differential stress values $(\sigma_1 - \sigma_3)$ were always calculated for a constant threshold $\tau_s = 10$ MPa. Generally, acceptable results were obtained with this assumption (e.g. Lacombe and Laurent, 1996, Table 1) but for one sample of Carrara marble in this last paper, an overestimation of 440% was calculated. This anomalous value was attributed

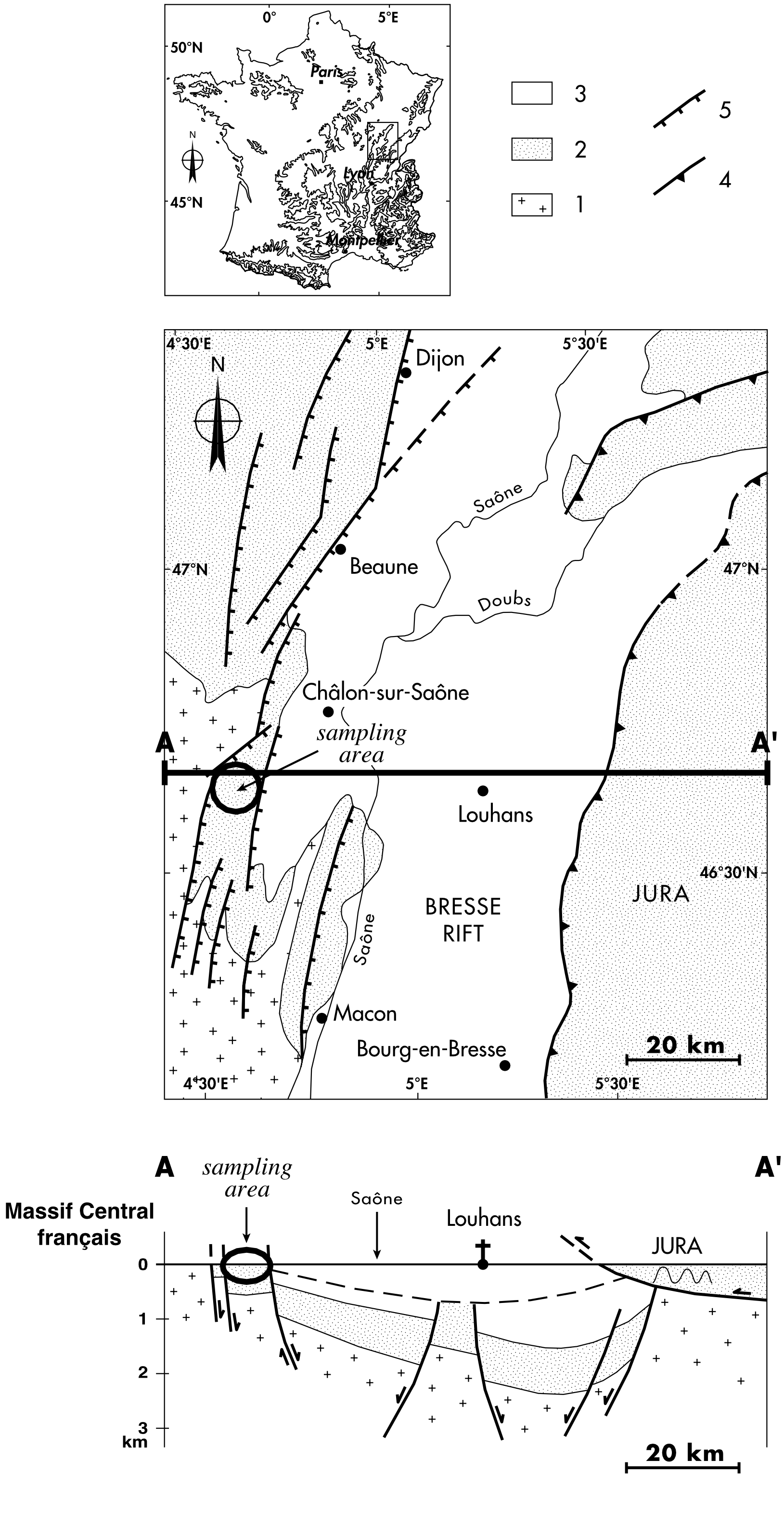
0°
5°E
50°N
Paris
Lyon
45°N
Montpellier
N
3
2
1
5
4
4°30'E
5°E
5°30'E
Dijon
N
Saône
Beaune
47°N
47°N
Doubs
Châlon-sur-Saône
sampling
area
A
A'
Louhans
46°30'N
BRESSE
RIFT
JURA
Saône
Macon
Bourg-en-Bresse
20 km
4°30'E
5°E
5°30'E
A
sampling
area
A'
Massif Central
français
Saône
Louhans
JURA
0
1
2
3
km
20 km

to too few untwinned planes to constrain the calculation of the DST. This point will be discussed later in the section concerning the sample B21.

5. Sampling and geological data

For our analysis, we chose a homogeneous poorly deformed sparitic limestone, without any shape or C axis preferred orientation of the calcite grains. Five samples (B1–B5) of a bajocian biosparitic grainstone were selected from five quarries situated on the eastern border of the Massif Central, about 15 km SW of Châlon Sur Saône (Fig. 3). In this area, the bedding plane S_0 dips gently to the West (N160E, 10W), and is locally affected by numerous N020E to N035E striking normal faults which are contemporaneous with the Bresse rifting. Locally, along these normal faults, fine breccias with centimetric angular blocks are cemented with white or pink clear calcite. Associated microstructures such as stylolitic peaks and subvertical N010E to N025E tension gashes are common. Although well expressed in the field, this extensional phase, probably related to the Oligocene extension of the Bresse basin, is not the only deformational phase: Two distinct sets of horizontal stylolitic peaks (respectively, NNE–SSW and NW–SE) were locally observed. The first set, classically attributed to the upper Eocene compressive "Pyrenean" phase (Bergerat, 1977), are sometimes associated with strike-slip faults (N010E to N035E, sinistral) that clearly predate the normal faults. The second set, generally poorly expressed in the studied area, may result from a Mio-Pliocene "Alpine" compressive phase related to thrusting of the Jura fold and thrust belt onto the Bresse basin (Fig. 3). For a general interpretation of the tectonics of the Bresse Basin, see Bergerat et al. (1990).

Regarded on thin section scale, bioclasts (echinoid spines, bryozoans and mollusks) are often overgrown by a syntaxial cement rim composed of a sparry calcite monocrystal. The pores between the grains were later filled with a cement composed of large euhedral transparent isodiametric calcite grains.

Some rare deformational microstructures were observed in the sample thin sections: (1) Stylolitic peaks. The peaks are oriented either perpendicular to the bedding plane S_0 (the most abundant) or strike N105E to N140E. (2) *e* twin lamellae in the calcite grains. They are straight and thin (about 0.5 μm in width) and traverse the crystal. These distinctive features lead us to interpret these *e* twin lamellae as the result of a low temperature deformation (Burkhard, 1993). In the different samples, the average twin density and the percentage of twinned crystals are very low, less than 10 per mm and 11–25% respectively. Most of the crystals (92%) are twinned on only one *e* set. Then, the natural deformation of the samples is very low, probably lower than 0.5%.

A set of three mutually orthogonal thin sections was made to study the calcite twins orientation and the *C* axis fabrics into the natural sample and the experimentally deformed ones.

6. Experimental deformation

The experiments were carried out in a triaxial pressure apparatus, designed in Kiel and described by Kern (1971, 1979).

Three approximately cubic samples with between 42.5 and 45.1 mm lengths were cut (Fig. 4). Two opposite faces of the cubes were cut parallel to the stratification plane S_0. The initial length is determined to a precision of 10^{-3} mm. The six cube faces were polished and covered with a thin coat of graphite to prevent displacement parallel to these faces. The bedding plane S_0 is normal to the principal axis of compression σ_1. The three dry specimens were heated indirectly by the pistons; a very homogeneous distribution of temperature to within 1°C was obtained

Fig. 3. Geological sampling. The middle of this figure is a very simplified geological map of the Bresse Rift, drawn from the Geological Map of France, at 1/1000.000 (1996). The location and legends are: (1) Paleozoic formations of the French Massif Central; (2) Mesozoic formations, essentially Trias to lower Cretaceous; (3) Tertiary to Quaternary formations of the Bresse Rift, with a thick pile (about one kilometer) of lower to mid Oligocene to the Eastern part of the rift; (4) Westward to Northward thrust of the folded Jura Massif on the Bresse Rift; (5) Normal faults; AA′ locates the simplified cross-section (after Rat, 1974). The dashed line of this cross-section corresponds to the upper Oligocene formation.

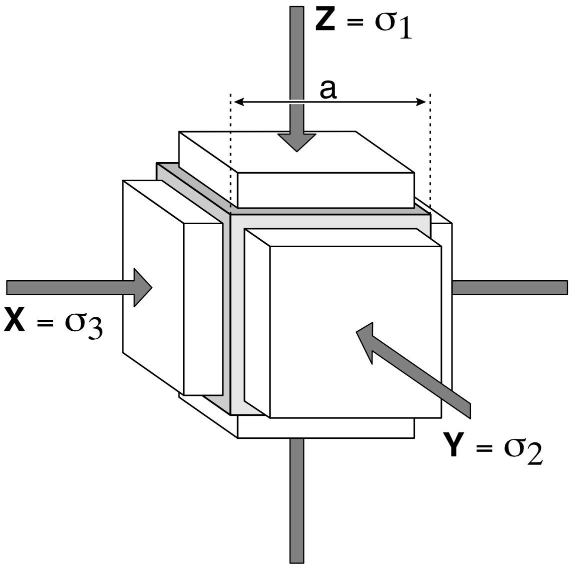

Fig. 4. Diagram illustrating the arrangement of the rock sample within the three couples of pistons. a is the initial length of the cube sample. It is close to 45 mm. For axial strain (B21 and B31), $\sigma_3 = \sigma_2$ the confining pressure P_c; for plane strain (B32), only $\sigma_3 =$ the confining pressure P_c (Table 1).

within the samples. The longitudinal strain $\Delta l/l$ is determined from the measurement of the piston displacement, using four sensors on each cube side. The estimated precision of the displacement is about 5×10^{-3} mm. The applied principal stresses, σ_i, are calculated and corrected for displacements normal to σ_1, σ_2 and σ_3. The estimated precision is about 5 MPa. The experiments are basically divided into three steps (summary of experimental conditions in Table 1).

Firstly, hydrostatic pressure is progressively increased, at room temperature, up to the chosen confining pressure P_c. Secondly, the samples are heated gradually, at constant confining pressure. Lastly, a load is applied at constant confining pressure and temperature (Fig. 5 and Tables 3–5).

The two samples B21 and B31 have been subjected to axial stress, with $\sigma_2 = \sigma_3 = P_c$. The sample B32 has been subjected to plane strain conditions, with $\epsilon_2 = 0$ on Y. In this last sample (Fig. 6), the SESR Φ has increased irregularly at the beginning of the experiment, from 0 to 0.4 ± 0.02; then, this value was almost constant (0.43 for the peak of differential stress $(\sigma_1 - \sigma_3)$).

7. Interpretation of experimental deformation

For the three experiments, the stress/strain curves were divided into three stages (I–III) (Table 2 and Fig. 5). The comparison of the data was made possible by normalizing the strain and stress parameters for a constant 100 MPa increase of the differential stress $(\sigma_1 - \sigma_3)$.

7.1. Stage I

At the beginning of the experiments, a very linear relationship between ϵ_1 and $(\sigma_1 - \sigma_3)$ is observed. This stage corresponds to a differential stress value $(\sigma_1 - \sigma_3)$ between 0 and 80 MPa. For the three samples, the SESR Φ remains equal to 0 $(\sigma_2 = \sigma_3)$. The normalized linear strain is about 0.4% for ϵ_1 and 0.01–0.03% for ϵ_2 and ϵ_3, respectively. The normalized average volume change $\Delta V/V$ is very low: −0.3 to −0.47%.

This deformation may be interpreted as essentially elastic with a calculated Young's modulus E equal to 26.3 ± 1.5 GPa. In Fig. 5, the CRSS values for twinning on e and gliding on r, according to Turner and Heard (1965) and De Bresser and Spiers (1997) have

Table 2
Interpretation of experimental deformation data

	I: Elastic $(0 \leq (\sigma_1 - \sigma_3) \leq 80$ MPa)	II: Transition $(80 \leq (\sigma_1 - \sigma_3) \leq 155$ MPa)
Normalized ϵ_1 (10^{-3})	−3.6 to −4	−7 to −9.5
Strain rate (10^{-7} s^{-1})	2.3–3	6–12.5
Normalized $\Delta V/V$ (10^{-3})	−3.32 to −4.7	−5.1 to −5.7
Young's modulus E (GPa)	26.3 ± 1.5	12.3 ± 1.9
Poisson's ratio ν	0.03–0.13	0.12–0.24

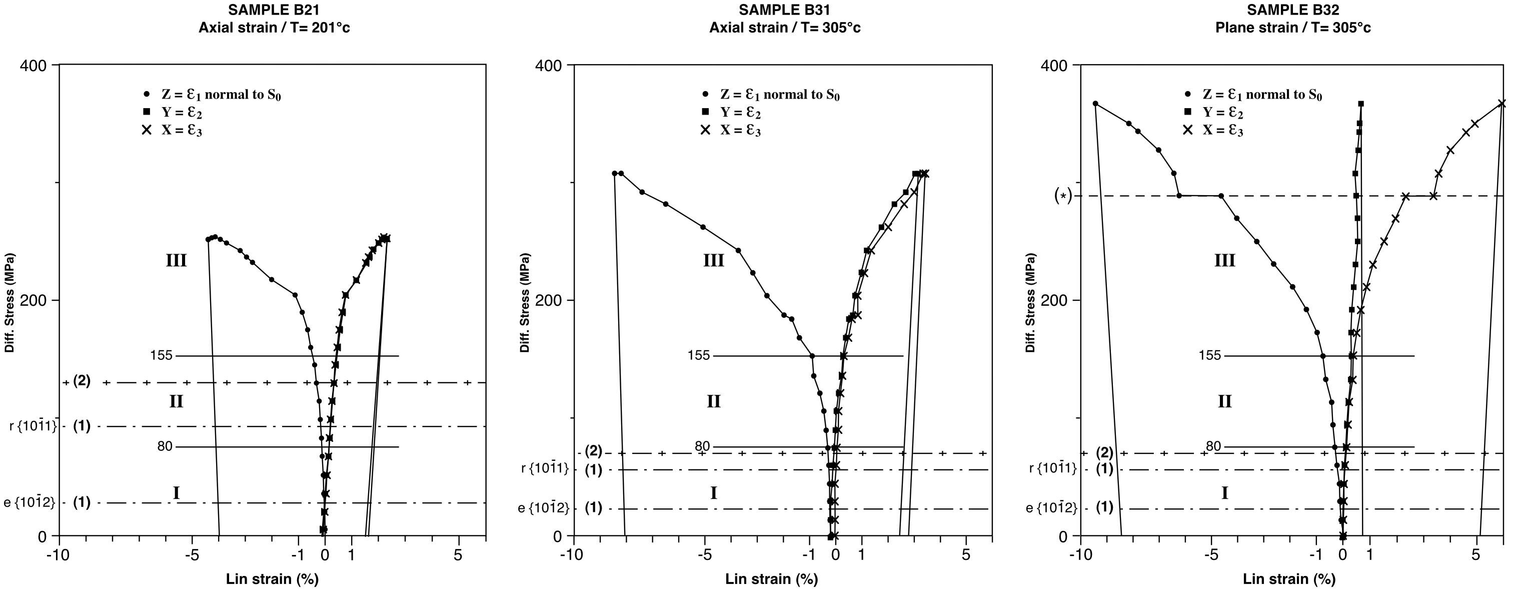

Fig. 5. Linear strain versus principal differential stress ($\sigma_1 - \sigma_3$) for the three samples B21, B31 and B32. I–III are the successive stages of deformation defined in the text; Dashed lines (1) correspond to the minimum values of the principal differential stress ($\sigma_1 - \sigma_3$) for twinning on *e* at yield, and for gliding on *r*, according to Turner et al. (1954). Dashed line (2) corresponds to the minimum value of the principal differential stress ($\sigma_1 - \sigma_3$) for gliding on *r*, after De Bresser and Spiers (1997) (extrapolated from their Fig. 6). Dashed line ($*$) corresponds to steady-state creep during the night.

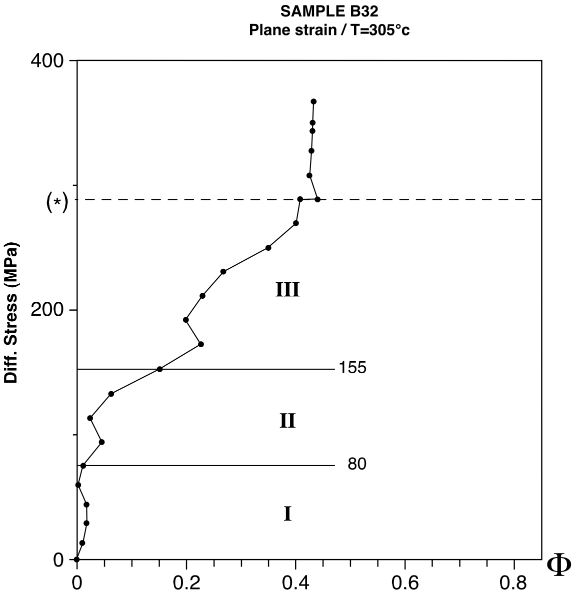

Fig. 6. Diagram of stress ellipsoid shape ratio (SESR) F values versus principal differential stress ($\sigma_1 - \sigma_3$) for the sample B32 (plane strain). I–III are the successive stages of deformation defined in the text. Dashed line (*) corresponds to steady-state creep during the night.

been reported (straight lines 1 and 2, respectively). It is therefore likely that twinning on the most favorable oriented calcite grains, may begin very early during the deformation process, i.e. before the end of this elastic deformation. At 300°C, gliding onto the *r* planes may also be possible for some well-oriented calcite grains.

7.2. Stage II

This second part is characterized by a different mean slope of the strain/stress curves (Fig. 5); it corresponds to a domain of differential stress values ($\sigma_1 - \sigma_3$) from 80 to 155 MPa. This stage is characterized by a nearly linear relationship between ϵ_1 and ($\sigma_1 - \sigma_3$) and quasi-axial stress conditions. Young's modulus E is about half the previous one and the linear strain rate is three to four times the previously calculated one.

7.3. Stage III

The last part of the strain/stress curves corresponds to a characteristic ductile behavior. The linear deformation ϵ_1 increases exponentially from about -1 to -4.83; -8.73 and -9.38% in B21, B31 and B32,

Table 3
Sample B21. 123 crystals. Twinned planes: 234 (63.4%); untwinned planes: 135 (36.6%). legend: %(1), percentage P of twinned planes, compatible with the RST; %(2), percentage of untwinned planes, incompatible with the RST. S_{UT}, maximal value of the RST τ_i for the untwinned planes incompatible with the RST; $\theta\sigma_1$, angle in degrees between the experimental principal stress axis σ_1 and the calculated one; Φ, calculated value of the SESR (theoretical $\Phi = 0$); F, value of the penalization function (see text); τ_a, minimal value of the resolved shear stresses τ_i for the twinned planes compatible with the RST. This value, theoretically always positive, is used to calculate the critical resolved shear stress τ_s (see text); CRSS $= \tau_s$, calculated value of the critical resolved shear stress for twinning on *e*, in MPa; $\tau_s = \tau_a(\sigma_1 - \sigma_3)$; * , absurdity, the resolved shear stress τ_a is negative. This means that some *e* planes, compatible with the RST, are twinned in the negative sense. Interpretation: best solution is for 72% of compatible twins. a, b, c and d are acceptable solutions (for discussion, see text)

%(1)	%(2)	S_{UT}	$\theta\sigma_1$	Φ	F	τ_a	CRSS	Interpretation
70	14.8	0.326	04	0.169	1.60	0.0695	17.236	
71	14.0	0.399	04	0.096	1.77	0.0540	13.392	a
71	14.0	0.403	05	0.060	1.81	0.0543	13.466	b
72	11.8	0.384	03	0.052	1.78	0.0529	13.119	c
72	16.3	0.361	03	0.133	1.69	0.0606	15.029	Best solution
73	14.8	0.323	04	0.159	1.82	0.0589	14.607	d
74	21.5	0.351	05	0.118	2.14	0.0414	10.267	
75	20.8	0.344	03	0.103	2.19	0.0371	9.20	
76	20.8	0.351	03	0.124	2.30	0.0358	8.88	
77	23.7	0.355	04	0.119	2.49	0.0292	7.24	
78	23.0	0.382	06	0.126	2.76	0.0221	5.46	
79	31.8	0.420	06	0.059	3.33	0.0001	0.025	
80	41.5	0.381	18	0.058	3.80	− 0.0565	*	

Table 4
Sample B31. Same legend as for Table 3. 145 crystals; twinned planes 342 (78.6%); untwinned planes 93 (21.4%). Interpretation: best solution is for 49% of compatible twins. a and b are acceptable solutions (for details, see text)

%(1)	%(2)	S_{UT}	$\theta\sigma_1$	Φ	F	τ_a	CRSS	Interpretation
45	0	–	09	0.037	0	0.0579	15.46	
46	1	0.068	08	0.041	0.02	0.0521	13.91	
47	2	0.064	10	0.014	0.02	0.0432	11.53	
48	0	–	07	0.202	0	0.0391	14.44	a
49	1	0.039	04	0.202	0	0.0380	10.15	Best solution
50	1	0.050	04	0.238	0.02	0.0337	9.0	b
51	2	0.067	07	0.108	0.06	0.0268	7.16	
52	3	0.075	07	0.129	0.08	0.0220	5.87	
53	4	0.049	04	0.157	0.10	0.0081	2.16	
54	3	0.060	08	0.579	0.11	− 0.0023	*	

respectively. The SESR Φ value increases from 0.2 to 0.4 (Fig. 6).

8. Inverse calculation of the RST

Tables 3–5 show the different parameters that will be used to define the best solutions. These parameters are: (1) The percentage P of e twin lamellae compatible with the RST. (2) The percentage of untwinned planes incompatible with the RST. (3) The maximum value (S_{uT}) of the resolved shear stress τ_i applied on the untwinned planes incompatible with the RST. (4) The value of the penalization function F. This last parameter indicates the quality of the arrangement of the whole measured e planes (for details, see Lacombe and Laurent, 1996). Only the computed RST corresponding to the experimental deformation (Fig. 7) will be mentioned in this paper.

The interpretation of these parameters leads to the definition of the RST best solutions, and the acceptable RST solutions. In the three studied samples, three

Table 5
Sample B32. Same legend as for Table 3. 94 crystals; twinned planes 240 (85%); untwinned planes 42 (15%). $\theta\sigma_3$, angle in degrees between the experimental principal stress axis σ_3 and the calculated one; the theoretical Φ value is 0.43. Interpretation: best solution is for 52% of compatible twins; a and b are acceptable solutions (for details, see text)

%(1)	%(2)	S_{UT}	$\theta\sigma_1$	$\theta\sigma_3$	Φ	F	τ_a	CRSS	Interpretation
47	0	–	04	06	0.312	0	0.0569	18.0	
48	4.8	0.090	05	06	0.284	0.01	0.0540	17.1	
49	4.8	0.063	04	06	0.301	0.01	0.0534	16.9	a
50	4.8	0.084	06	10	0.308	0.03	0.0519	16.4	b
51	7.1	0.098	11	09	0.405	0.09	0.0532	16.8	
52	7.1	0.070	07	11	0.384	0.04	0.0424	13.4	Best solution
53	4.8	0.136	10	10	0.398	0.13	0.0449	14.2	
54	16.7	0.072	05	12	0.324	0.13	0.0241	7.62	
55	11.9	0.079	07	09	0.363	0.16	0.0186	5.88	
56	7.1	0.140	05	11	0.338	0.17	0.0239	7.55	
57	9.5	0.123	01	10	0.283	0.20	0.0133	4.2	
58	11.9	0.108	02	17	0.295	0.23	0.0145	4.58	
59	11.9	0.111	02	16	0.302	0.24	0.0110	3.47	
60	19	0.114	01	14	0.311	0.31	− 0.0059	*	
70	33.3	0.145	06	21	0.172	1.04	− 0.0567	*	

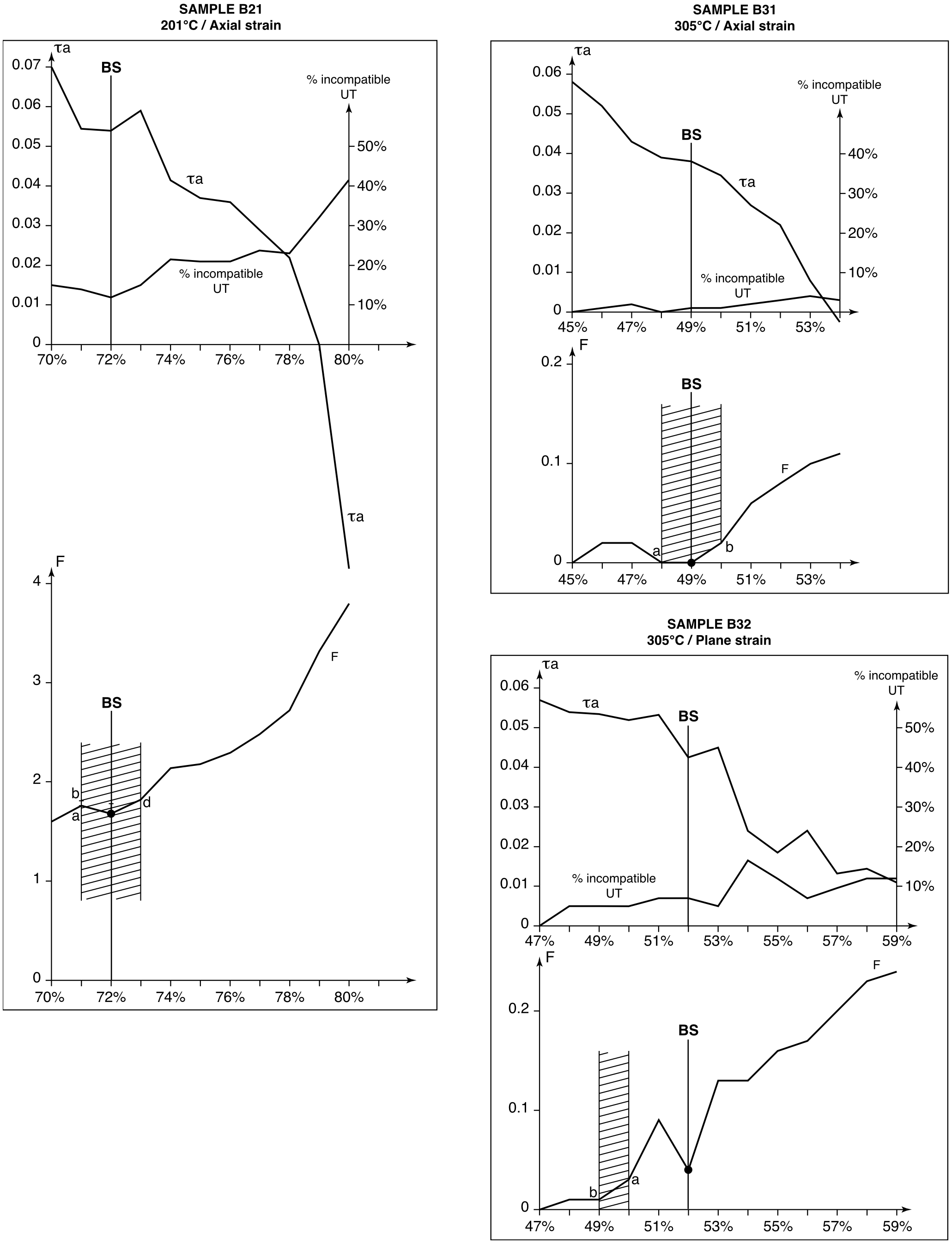

Fig. 7. Definition of the RST best solutions (indicated by the vertical lines BS) in the three samples B21 (left of this figure), B31 (upper right) and B32 (lower right). On the upper part, are the diagrams of τ_a versus the percentage P of compatible twin planes (horizontal axis); τ_a is the minimum value of the resolved shear stress τ_i for the twinned planes compatible with the best RST solution (vertical axis on the left); on the same diagram, the percentage of incompatible untwinned planes is also drawn (vertical axis on the right). Underneath, are the diagrams of the penalization function F (vertical axis) versus the percentage P of compatible twin planes (horizontal axis). a–d and the shaded areas are the acceptable solutions defined in Tables 3–5.

to five RST solutions are considered to be acceptable which define the interval of confidence for the different parameters of the calculated DST.

Tables 3–5 also indicate: (1) The angle between the computed principal stress axis σ_1 (σ_1 and σ_3 in the case of B32) and the experimental one(s). (2) The computed SESR Φ values. (3) The minimum value τ_a of the resolved shear stresses τ_i applied on the twinned planes compatible with the RST (see also Fig. 7). These τ_a values are used to calculate the CRSS τ_s for twinning on *e*:

$$\tau_s = \tau_a(\sigma_1 - \sigma_3) \tag{2}$$

8.1. Sample B21: axial stress; T = 201°C

In this sample 36.6% of the measured *e* planes are untwinned. This relatively high value is probably linked to the low final linear strain ϵ_1 (less than 5%). When no preferred orientation of the calcite grains is observed, such a high percentage of untwinned planes is always correlated with a high percentage of classified incompatible untwinned planes (Table 3; column 2); then the penalization function value F is much higher for B21 than for B31 and B32. The two main reasons that may account for this are: (1) The effective CRSS value which actually depends on the amount of strain (see discussion below). (2) The greater heterogeneity of strain (and stress) in the low deformed samples, due to the large mechanical anisotropy of the calcite crystals (see also Spiers, 1979).

Table 3 shows 13 trials which correspond to an increasing percentage P comprised between 70 and 80%. If we reject the last line ($P = 80\%$), which is clearly a wrong solution (τ_a is negative), one may observe that: (1) the computed stress tensor orientation is defined quite precisely as 3–6°; it is the same order of precision as that of the making of the thin sections (particularly the sawing process); (2) the SESR Φ value is much more variable, from about 0.05 to about 0.17; (3) The F value increases more or less regularly with the percentage P.

The best computed inverse solution is defined for $P = 72\%$. The percentage of incompatible untwinned planes is relatively high, with respect to the solutions which are close to it (a–d); this means that the arrangement of these incompatible untwinned planes is such that they are situated more on the left in the diagram of Fig. 2b (see also Fig. 8). A comparison of the two RST calculated with $P = 72\%$ (the best solution and solution c in Table 3), shows that the best solution is essentially due to a different Φ value (0.133 in place of 0.052).

Considering the best solution and the acceptable ones, the results may be summarized as follows: (1) the principal stress direction σ_1 is at 3–5 from the theoretical one; (2) the SESR Φ value is equal to 0.13 (+0.03; −0.08); for the best solution ($\Phi = 0.133$), the calculated σ_2 value is 135 MPa, which corresponds to an overestimation of 32.5%; (3) the τ_a value is equal to 0.0606 (+0; −0.007); as the maximum of the applied differential stress ($\sigma_1 - \sigma_3$) was equal to 248 MPa (Table 1), the computed CRSS for twinning on *e* (Fig. 9) is about 15 MPa (+0; −1.6).

8.2. Sample B31: axial stress; T = 305°C

In sample B31, the best solution is defined for $P = 49\%$ and two acceptable solutions are found for $P = 48$ and 50% (see Table 4 and Fig. 8). (1) The principal stress direction σ_1 is at 4–7° from the theoretical one. (2) The SESR Φ value is equal to 0.2 (+0.04; −0); 3) the τ_a value is equal to 0.038 (+0.001; −0.005). Then, using Eq. (2) and the actual value of ($\sigma_1 - \sigma_3$), i.e. 267 MPa, the computed CRSS for twinning on *e* (Fig. 9) is equal to 10.1 MPa (+0.5; −1).

As for sample B21, the precision of the principal stress direction σ_1 is good, but the SESR Φ value is very variable for the different trials. For the best solution ($\Phi = 0.202$), the calculated σ_2 value is 267 MPa, which corresponds to an overestimation of 25%.

8.3. Sample B32: triaxial stress; T = 305°C

In sample B32, the best solution is defined for $P = 52\%$; and two acceptable solutions are described for $P = 49$ and 50%. (Table 5 and Fig. 8). (1) The principal stress direction σ_1 is at 4–7° from the theoretical one. (2) The principal stress direction σ_3 is at 6–11° from the theoretical one. (3) The SESR Φ value is equal to 0.384 (+0; −0.08) which corresponds to an underestimation of about 12%. (4) The τ_a value is equal to 0.0424 (+0.011; −0). Then, using Eq. (2) and the actual value of ($\sigma_1 - \sigma_3$), i.e. 316 MPa, the computed CRSS for twinning on *e* (see Fig. 9) is equal to 13.4 MPa (+3.5; −0).

9. Discussion of the results

The calculated principal stress orientations show very stable solutions from one RST solution to the other (Tables 3–5). They correspond within a few degrees to the experimental ones. Although this result was predictable for axial stress (Lacombe and Laurent, 1996), it is the first time that plane strain conditions are used for the inverse analysis. The results concerning the sample B32 show that the principal intermediate stress σ_2 is well determined.

In a first approach, the magnitude of the principal differential stresses ($\sigma_1 - \sigma_3$) was calculated according to the hypothesis used up till now, that the CRSS value τ_s is constant and equals 10 MPa. For the best solutions, we obtained: 165, 263 and 236 MPa for B21, B31 and B32, respectively. Compared to the peak of applied differential stress ($\sigma_1 - \sigma_3$) (Table 1), these values are underestimated by 33.5, 1.5 and 25.5%, respectively. If we take into account the acceptable solutions, the range of variation for the ($\sigma_1 - \sigma_3$) values is: −33.5 to −23.8% for B21; −4 to +11% for B31; and −25.5 to −41% for B32. Thus, these three experiments carried out at 200 and 300°C lead to a general underestimation of the ($\sigma_1 - \sigma_3$) values by about 40%.

The calculation of the two differential stress magnitudes ($\sigma_2 - \sigma_3$) and ($\sigma_1 - \sigma_2$), from Eq. (2) and the SESR Φ value shows that: (1) For axial stress ($\Phi = 0$), the results are rather unstable (Tables 3 and 4). This is probably related to the fact that the minimization process of the Etchecopar inverse method is mainly dependent on the incompatible untwinned planes; consequently, the orientation fabrics of the untwinned planes must influence these results. (2) For triaxial stress, the results are very close to the expected ones (Table 5). As it is the first time that experimental triaxial stress is analyzed using an

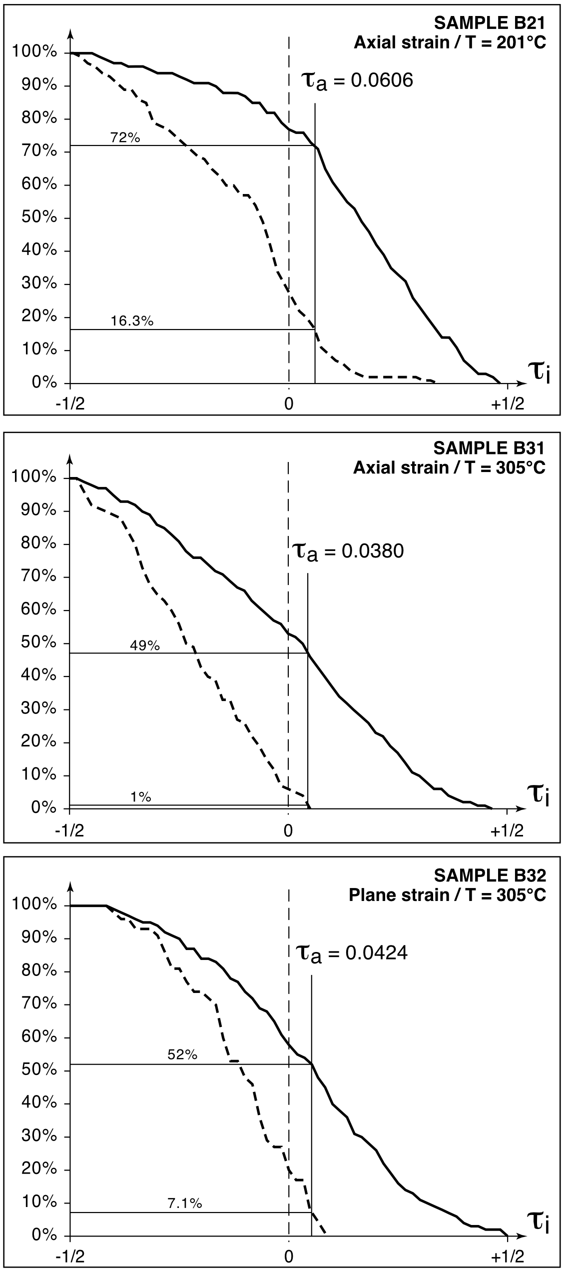

Fig. 8. Classification of the whole set of *e* planes (twinned and untwinned) with respect to the applied resolved shear stress τ_i computed from the best RST solutions for the samples B21, B31 and B32. On the horizontal axes, are the resolved shear stress τ_i values, in the range −0.5 to +0.5 from left to right of the diagram. On the vertical axes, are the percentages of classified *e* planes (continuous curves, twinned planes; dashed curves, untwinned planes). τ_a is the minimum value of the resolved shear stress τ_i for the whole set of compatible twin planes. Percentages of compatible twinned planes (upper horizontal lines)/respectively incompatible untwinned planes (lower horizontal lines) are indicated for the three samples.

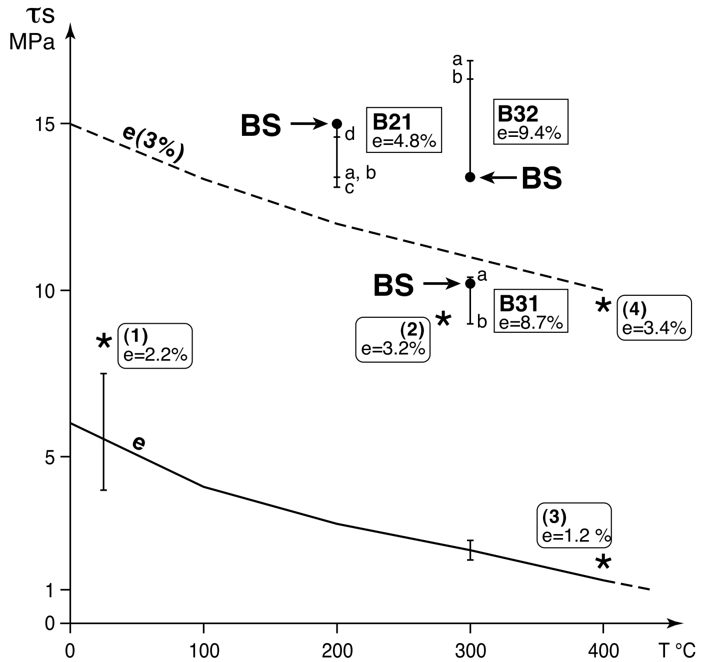

Fig. 9. Diagram of the critical resolved shear stress (CRSS) values τ_s for twinning on *e* as a function of temperature and strain. *Previous work:* Continuous line: values calculated at yield (incipient twinning), after Turner et al. (1954). Dashed line: values calculated at 3% strain, after Turner and Heard (1965). Crosses: values calculated from the experimental deformation of Lacombe and Laurent (1996). 1 is a crinoidic limestone very comparable with the samples used in this paper ($\tau_s = 8.5$ MPa for 2.2% strain at room temperature); 2–4 correspond to Carrara marbles (τ_s is ,respectively, equal to: 9.13 (this value has been recalculated by Rocher (1999) from the original data set), 1.85 and 9.63 MPa for 3.2, 1.2 and 3.4% strain; the temperature of deformation is 280°C for sample 2, and 400°C for the samples 3 and 4). *This paper:* B21, B31 and B32 are the values determined in this paper; a–d are the different acceptable solutions; BS are the best solutions.

inverse method, further data are needed to draw definite conclusions because, as in the previous cases, the fabrics of incompatible untwinned planes should influence this result.

An alternative use of these experimental data has been the calculation of the CRSS values τ_s for twinning on *e* from Eq. (2) and the actual values of $(\sigma_1 - \sigma_3)$. These τ_s values have been plotted in Fig. 9, together with those of Turner et al. (1954), Turner and Heard (1965) and Lacombe and Laurent (1996). For each sample, the percentage of strain is indicated. The continuous line of the Fig. 9 is defined at yield, which probably corresponds to the maximum shearing stresses at which twinning is initiated (Carter, 1976). The dashed line of the Fig. 9 is calculated for 3% of finite strain. These two curves show that the CRSS values τ_s for twinning on *e* are strain dependent. That strain dependence is linked to the fact that twinning is very sensitive to the presence of inhomogeneities within the crystals (Schmid and Boas, 1950). Thus, during the deformation process, twinning must get more and more difficult with the increase of strain and the resolved shear stress value necessary to twin the worst oriented *e* planes (i.e. the value which defines the CRSS value τ_s for twinning on *e*), will increase with strain. This may explain the fact that in the higher deformed samples the principal differential stress values $(\sigma_1 - \sigma_3)$, calculated using a constant 10 MPa value for τ_s, are generally underestimated. In our deformed samples, twinning has been achieved probably as early as the first stage of deformation (I in Fig. 6), within the calcite grains which were the most favorably oriented. Then, during stages II and III, twinning on *e* may have developed into more and more calcite grains, even when the gliding on the *r* planes should have become an easier mechanism for the deformation (Fig. 5).

The consequences of these results on the determination of principal differential stress values for geological cases, particularly in the foreland of mountain chains (e.g. Lacombe and Laurent, 1991, 1996; Craddock et al., 1993; Van Der Pluijm et al., 1997) may be summarized as follows: for the low strained sparitic limestones (i.e. strain lower than about 1.5%), the CRSS value τ_s for twinning on *e* which may be used is more likely about that proposed by Turner et al. (1954) for incipient twinning: at room temperature, it is about 5–7 MPa. As a result, the previous determinations of $(\sigma_1 - \sigma_3)$ in the foreland of the Pyrenean chain (Tourneret and Laurent, 1990; Lacombe et al., 1991, 1996; Lacombe and Laurent, 1992) may have been overestimated by a factor in the range 1.43–2.

10. Conclusions

This experimental work confirms that: (1) inverse determination of DST gives reliable results for the principal stress orientations, even when the state of stress is triaxial; (2) the CRSS values τ_s for twinning on *e* in calcite grain are mainly dependent on both temperature and strain (an increase of temperature/strain respectively lowers/increases the τ_s values). For limestones strained to about 5–10%, the τ_s values are circa 10–15 Mpa at 200 and 300°C.

On the other hand, this work confirms that the τ_s value proposed by Turner et al. (1954) for incipient twinning, i.e. 5–7 MPa, is more likely for slightly deformed limestones.

The use of the Etchecopar method (1984) together with the correct values of τ_s defined in Fig. 9, should lead to the magnitude of $(\sigma_1 - \sigma_3)$ with an interval of confidence estimated at about 50%. This is much better than the overestimation by a factor up to 20, obtained with the methods of Jamison and Spang (1976) and Rowe and Rutter (1990) by Ferrill (1998). In order to confirm these results for the application to the paleostress fields associated with the tectonics of mountain forelands, further experiments, particularly at low temperatures (0–200°C) and low strain (0–2%), are needed to support these results.

Acknowledgements

This work was supported by a "programme d'actions intégrées" PROCOPE. We wish to thank J.P. Burg from the ETH Zürich, for the improvement of this manuscript. Special thanks go to Dana Petit for the revision of the English version, to Anne Delplanque for the drawings and M. Peret for help in data processing. K. Burmeister prepared the samples and M. Schroetel assisted in performing the experiments. The thin sections were made by L. Cammal.

References

Angelier, J., 1984. Tectonic analysis of fault slip data sets. J. Geophys. Res. 89, 5835–5848.

Angelier, J., 1989. From orientation to magnitudes in paleostress determinations using fault slip data. J. Struct. Geol. 11, 37–50.

Arthaud, F., Laurent, Ph., 1995. Contraintes, déformation et déplacement dans l'avant-pays Nord-pyrénéen du Languedoc méditerranéen. Geodinam. Acta 8, 142–157.

Barber, D.J., Wenk, H.R., 1979. Deformation twinning in calcite, dolomite and other rhombohedral carbonates. Phys. Chem. Miner. 5, 141–165.

Bergerat, F., 1977. La fracturation de l'avant-pays jurassien entre les fossés de la Saône et du Rhin. Analyse et essai d'interprétation dynamique. Rev. Géogr. Phys. Géol. Dynam. Paris 19, 325–338.

Bergerat, F., Mugnier, J.L., Guellec, S., Truffert, C., Cazes, M., Damotte, B., Roure, F., 1990. Extensional tectonics and subsidence of the Bresse basin: an interpretation from ECORS data. Mém. Soc. Géol. Fr. 156, 145–156.

Bott, M.H.P., 1959. The mechanics of oblique slip faulting. Geol. Mag. 96, 109–117.

Burkhard, M., 1993. Calcite twins, their geometry, appearance and significance as stress–strain markers and indicators of tectonic regime: a review. J. Struct. Geol. 15, 351–368.

Cahn, R.W., 1954. Twinned crystals. Advances in physics. Philos. Mag. 3, 363–445.

Carter, N.L., 1976. Steady state flow of rocks. Reviews of geophysics and space physics. J. Geophys. Res. 14 (3), 301–359.

Carter, N.L., Raleigh, C.B., 1969. Principal stress directions from plastic flow in crystals. Geol. Soc. Am. Bull. 80, 1231–1264.

Craddock, J.P., Jackson, M., Van Der Pluijm, B.A., Versical, R.T., 1993. Regional shortening fabrics in Eastern North America: far field stress transmission from the Appalachian–Ouachita orogenic belt. Tectonics 12, 257–264.

De Bresser, J.H.P., Spiers, C.J., 1993. Slip systems in calcite single crystals deformed at 300–800°C. J. Geophys. Res. 98, 6397–6409.

De Bresser, J.H.P., Spiers, C.J., 1997. Strength characteristics of the r, f and c slip systems in calcite. Tectonophysics 272, 1–23.

Engelder, T., Geiser, P., 1980. On the use of regional joint sets as trajectories of paleostress fields during the development of the

Appalachian plateau, New York. J. Geophys. Res. 85, 6319–6341.

Etchecopar, A., 1984. Etude des états de contrainte en tectonique cassante et simulation de déformations plastiques (approche mathématique). Thesis, Univ. Sci. Technique du Languedoc, Montpellier, 270pp.

Etchecopar, A., Vasseur, G., Daignieres, M., 1981. An inverse problem in microtectonics for the determination of stress tensors from fault striation analysis. J. Struct. Geol. 3, 51–65.

Ferrill, D.A., 1998. Calcite twin width and intensities as metamorphic indicators in natural low-temperature deformation of limestone. J. Struct. Geol. 13, 667–675.

Friedel, G., 1926. Leçons de cristallographie. Berger-Levrault, Paris (602pp.).

Friedman, M., 1967. Description of rocks and rock masses with a view to their physical and mechanical behavior. Proceedings of the 1st International Congress on Rock Mechanics, vol. 3, pp. 182–197.

Friedman, M., Stearns, D.W., 1971. Relations between stresses inferred from calcite twin lamellae and macrofractures, Teton anticline, Montana. Bull. Geol. Soc. Am. 82, 3151–3162.

Friedman, M., Heard, H.C., 1974. Principal stress ratio in Cretaceous limestones from Texas Gulf Coast. Bull. Am. Assoc. Petrol. Geol. 58, 71–78.

Friedman, M., Teufel, L.W., Morse, J.D., 1976. Strain and stress analysis from calcite twin lamellae in experimental buckles and faulted drape-folds. Philos. Trans. R. Soc. 283, 87–107.

Geological Map of France at 1/1000.000, 1996. Bureau de Recherches Géologiques et Minières, sixième édition, Orléans: France.

Gonzalez-Casado, J.M., Garcia-Cuevas, C., 1999. Calcite twins from microveins as indicators of deformation history. J. Struct. Geol. 21, 875–889.

Jamison, W.R., Spang, J.H., 1976. Use of calcite twin lamellae to infer differential stress. Geol. Soc. Am. Bull. 87, 868–872.

Kern, H., 1971. Dreiaxiale verformungen an Solnhofen Kalkstein im Temperaturbereichvon 20–650°C Röntgenographische Gefügeuntersuchungen mit dem texturogoniometer. Contrib. Mineral. Petrol. 31, 39–66.

Kern, H., 1979. Texture development in calcite and quartz deformed at uniaxial and real triaxial states of strain. Bull. Mineral. 102, 290–300.

Lacombe, O., Angelier, J., Bergerat, F., Laurent, Ph., 1990a. Tectoniques superposées et perturbations de contraintes dans la zone transformante Rhin-Saône: apport de l'analyse des failles et des macles de la calcite. Bull Soc. Geol. Fr. VI/5, 853–863.

Lacombe, O., Angelier, J., Laurent, Ph., Bergerat, F., Tourneret, Ch., 1990b. Joint analyses of calcite twins and fault slips as a key for deciphering polyphase tectonics: Burgundy as a case sample. Tectonophysics 182, 279–300.

Lacombe, O., Bergues, J., Angelier, J., Laurent, Ph., 1991. Quantification des paléocontraintes à l'aide des macles de la calcite: l'exemple de la compression pyrénéo-provençale au front de la Montagne Sainte-Victoire (Provence). C.R. Acad. Sci. Paris 313, 1187–1194.

Lacombe, O., Laurent, Ph., 1991. Variation of deformation style and decreasing magnitude of tectonic stress north on the Pyrenean orogeny. International Conference on Mechanical Instabilities in Rocks and Tectonics, Montpellier. Terra Abstracts, supp. 5 to Terra Nova 3, p. 21.

Lacombe, O., Angelier, J., Laurent, Ph., 1992. Determining paleostress orientations from faults and calcite twins: a case study near the Sainte-Victoire range. Tectonophysics 201, 141–156.

Lacombe, O., Laurent, Ph., 1992. Determination of principal stress magnitudes using calcite twins and rock mechanics data. Tectonophysics 202, 83–97.

Lacombe, O., Angelier, J., Laurent, Ph., 1993. Les macles de la calcite, marqueurs des compressions récentes dans un orogène actif: l'exemple des calcaires récifaux du Sud de Taiwan. C.R. Acad. Sci. Paris 316, 1805–1813.

Lacombe, O., Laurent, Ph., Rocher, M., 1996. Magnitude de la contrainte déviatorique pyrénéenne dans l'avant-pays nord-pyrénéen. C.R. Acad. Sci. Paris (B) 322, 229–235.

Lacombe, O., Laurent, Ph., 1996. Determination of deviatoric stress tensors based on inversion of calcite twin data from experimentally deformed monophase samples. Preliminary results. Tectonophysics 255 (3/4), 189–202.

Larroque, J.M., Laurent, Ph., 1988. Evolution of the stress field pattern in the South of the Rhine graben from the Eocene to the present. Tectonophysics 148, 41–58.

Laurent, Ph., 1984. Les macles de la calcite en tectonique: nouvelles méthodes dynamiques et premières applications. Unpublished PhD thesis, Univ. Sci. Technique du Languedoc, Montpellier, 324pp.

Laurent, Ph., Bernard, Ph., Vasseur, G., Etchecopar, A., 1981. Stress tensor determination from the study of *e*-twins in calcite. A linear programming method. Tectonophysics 78 (1–4), 651–660.

Laurent, Ph., Tourneret, Ch., Laborde, O., 1990. Determining deviatoric stress tensors from calcite twins: applications to monophased synthetic and natural polycrystals. Tectonics 9 (3), 379–389.

Marrett, R., Peacock, D.C.P., 1999. Strain and stress. J. Struct. Geol. 21, 1057–1063.

Nemcock, M., Kovac, D., Lisle, R.J., 1999. A stress inversion procedure for polyphase calcite twin and fault/slip data sets. J. Struct. Geol. 21, 597–611.

Newman, J., 1994. The influence of grain size and grain size distribution on methods for estimating paleostresses from twinning in carbonates. J. Struct. Geol. 16, 1589–1601.

Olsson, W.A., 1974. Grain size dependence of yield stress in marble. J. Geophys. Res. 79, 4859–4862.

Rocher, M., 1999. Déformations et paléocontraintes des avant-pays de chaÎnes de collision: les piedmonts occidentaux de TaÏwan et le bassin Sud-Aquitain. Unpublished PhD thesis, Univ. Pierre et Marie Curie, Paris, 409pp.

Rat, P., 1974. Le système Bourgogne–Morvan–Bresse (articulation entre le bassin parisien et le domaine périalpin). In: Debelmas, J. (Ed.), Géologie de la France, vol. II: Les chaÎnes plissées du cycle alpin et leur avant-pays. Doin éditeurs: France, pp. 480–500.

Rowe, K.J., Rutter, E.H., 1990. Palaeostress estimation using calcite twinning: experimental calibration and application to nature. J. Struct. Geol. 12, 1–17.

Schmid, E., Boas, W., 1950. Plasticity of Crystals, with Special Reference to Metals. Chapman and Hall, London (353pp.).

Schmid, S.M., 1982. Microfabric studies as indicators of deformation mechanisms and flow laws operative in mountain building. In: Hsü, K.J. (Ed.). Mountain Building Processes. Academic Press, London, pp. 95–110.

Spiers, C.J., 1979. Fabric development in polycrystals deformed at 400°C. Bull. Mineral. 102, 282–289.

Tourneret, Ch., Laurent, Ph., 1990. Paleostress orientations from calcite twins in the North Pyrenean foreland by the Etchecopar inverse method. Tectonophysics 180, 287–302.

Tullis, T.E., 1980. The use of mechanical twinning in minerals as a measure of shear stress magnitudes. J. Geophys. Res. 85, 6263–6268.

Turner, F.J., 1953. Nature and dynamic interpretation of deformation lamellae in calcite of three marbles. Am. J. Sci. 251, 276–298.

Turner, F.J., 1962. “Compression” and “tension” axes determined from (0112) twinning in calcite. J. Geophys. Res. 67, 1660.

Turner, F.J., Griggs, D.T., Heard, H.C., 1954. Experimental deformation of calcite crystals. Geol. Soc. Am. Bull. 65, 883–934.

Turner, F.J., Heard, H.C., 1965. Deformation in calcite crystals at different strain rates. Geol. Sci. Publ. Univ. Calif. Los Angeles 46, 103–126.

Van Der Pluijm, B.A., Craddock, J.P., Graham, B.R., Harris, J.H., 1997. Paleostress in cratonic north America: implications for deformation of continental interiors. Science 277, 794–796.

Wallace, R.E., 1951. Geometry of shearing stress and relation to faulting, . J. Geol. 59, 118–130.

Wenk, H.R., Barber, D.J., Reeder, R.J., 1983. Microstructures in carbonates. In: Reeder, R.J. (Ed.), Carbonates: Mineralogy and Chemistry, vol. 11. Rev. Miner. Soc. Am., pp. 301–367.

Wheeler, J., 1991. A view of texture dynamics. Terra Nova 3, 123–136.

Zoback, M.L., 1992. First- and second-order patterns of stress in the lithosphère: the World Stress Map project. J. Geophys. Res. 97, 11703–11728.

Zoback, M.L., Zoback, M.D., Adams, J., Assumpçao, M., Bell, S., Bergman, E.A., Blümling, P., Brereton, N.R., Denham, D., Ding, J., Fuchs, K., Gay, N., Gregersen, S., Gupta, H.K., Gvishiani, A., Jacob, K., Klein, R., Knoll, P., Magee, M., Mercier, J.L., Müller, B.C., Paquin, C., Rajendran, K., Stephansson, O., Suarez, G., Suter, M., Udias, A., Xu, Z.H., Zhizhin, M., 1989. Global patterns of tectonic stress. Nature 341, 291–298.